Journal of Biomedical Optics

BiomedicalOptics.SPIEDigitalLibrary.org

In vivo evaluation of adipose- and muscle-derived stem cells as a treatment for nonhealing diabetic wounds using multimodal microscopy

Joanne Li
Yair Pincu
Marina Marjanovic
Andrew J. Bower
Eric J. Chaney
Tor Jensen
Marni D. Boppart
Stephen A. Boppart

SPIE.

Joanne Li, Yair Pincu, Marina Marjanovic, Andrew J. Bower, Eric J. Chaney, Tor Jensen, Marni D. Boppart, Stephen A. Boppart, "*In vivo* evaluation of adipose- and muscle-derived stem cells as a treatment for nonhealing diabetic wounds using multimodal microscopy," *J. Biomed. Opt.* **21**(8), 086006 (2016), doi: 10.1117/1.JBO.21.8.086006.

In vivo evaluation of adipose- and muscle-derived stem cells as a treatment for nonhealing diabetic wounds using multimodal microscopy

Joanne Li,[a,b] Yair Pincu,[a,c] Marina Marjanovic,[a,b] Andrew J. Bower,[a,d] Eric J. Chaney,[a] Tor Jensen,[e] Marni D. Boppart,[a,c] and Stephen A. Boppart[a,b,d,f,*]

[a]University of Illinois at Urbana-Champaign, Beckman Institute for Advanced Science and Technology, 405 North Mathews Avenue, Urbana, Illinois 61801, United States
[b]University of Illinois at Urbana-Champaign, Department of Bioengineering, 1270 Digital Computer Laboratory MC-278, 1304 West Springfield Avenue, Urbana, Illinois 61801, United States
[c]University of Illinois at Urbana-Champaign, Department of Kinesiology and Community Health, 906 South Goodwin Avenue, Urbana, Illinois 61801, United States
[d]University of Illinois at Urbana-Champaign, Department of Electrical and Computer Engineering, 306 North Wright Street, Urbana, Illinois 61801, United States
[e]University of Illinois at Urbana-Champaign, Illinois Health Sciences Initiative, 611 West Park Street, Urbana, Illinois 61801, United States
[f]University of Illinois at Urbana-Champaign, Department of Internal Medicine, 506 South Mathews Avenue, Urbana, Illinois 61801, United States

Abstract. Impaired skin wound healing is a significant comorbid condition of diabetes, which often results in nonhealing diabetic ulcers due to poor peripheral microcirculation, among other factors. The effectiveness of the regeneration of adipose-derived stem cells (ADSCs) and muscle-derived stem cells (MDSCs) was assessed using an integrated multimodal microscopy system equipped with two-photon fluorescence and second-harmonic generation imaging. These imaging modalities, integrated in a single platform for spatial and temporal coregistration, allowed us to monitor *in vivo* changes in the collagen network and cell dynamics in a skin wound. Fluorescently labeled ADSCs and MDSCs were applied topically to the wound bed of wild-type and diabetic (*db*/*db*) mice following punch biopsy. Longitudinal imaging demonstrated that ADSCs and MDSCs provided remarkable capacity for improved diabetic wound healing, and integrated microscopy revealed a more organized collagen remodeling in the wound bed of treated mice. The results from this study verify the regenerative capacity of stem cells toward healing and, with multimodal microscopy, provide insight regarding their impact on the skin microenvironment. The optical method outlined in this study, which has the potential for *in vivo* human use, may optimize the care and treatment of diabetic nonhealing wounds. [DOI: 10.1117/1.JBO.21.8.086006]

Keywords: microscopy; medical imaging; second-harmonic generation; fluorescence.

Paper 160248RR received Apr. 14, 2016; accepted for publication Jul. 28, 2016; published online Aug. 16, 2016.

1 Introduction

In recent years, over 29 million (9.3%) American adults were diagnosed with diabetes, with Type 2 diabetes accounting for 90% to 95% of all cases.[1] Insulin resistance and subsequent elevation of blood glucose can result in generation of reactive oxygen species and advanced glycation end products that destroy proteins necessary for vessel and nerve structure and function.[2] Microvessel and nerve damage provide the basis for the majority of chronic diseases and conditions associated with Type 2 diabetes, including cardiovascular and kidney diseases, retinopathy, glaucoma, peripheral neuropathy, and impaired skin wound healing.[3]

Impaired skin wound healing is a significant comorbid condition of diabetes. Diabetes-induced peripheral neuropathy results in an increased number of skin lesions that can progress to nonhealing ulcers, mainly because of poor peripheral microcirculation,[4] often leading to nontraumatic lower-limb amputations.[4] Therefore, there is a critical need to better understand the microscopic cell, tissue, and microvascular changes that occur in these nonhealing wounds and seek appropriate treatment for them.

Wound healing is a dynamic, interactive process that typically consists of three phases overlapping in time: inflammation, proliferation, and tissue remodeling.[5,6] During the inflammation phase, inflammatory cells including neutrophils and macrophages are recruited to the wound site to phagocytose the bacteria and dead cells in order to prepare the wound for healing.[5,7] Fibroblast migration and proliferation predominates the second phase, which also includes synthesis of collagen necessary for tissue repair, re-epithelialization of the epidermis, angiogenesis, and myofibroblast-mediated wound contraction and closure.[7,8] During the tissue remodeling phase, the deposition of extracellular matrix (ECM) takes place with appropriate collagen abundance and alignment.[5,8] Under diabetic conditions, changes in the immune response, including excessive neutrophil and macrophage influx, can disrupt the normal wound healing process.[9] In addition, abnormalities in the microvasculature often disrupt cell transportation and communication, causing complications

*Address all correspondence to: Stephen A. Boppart, E-mail: boppart@illinois.edu

1083-3668/2016/$25.00

in other wound healing events such as re-epithelialization and collagen formation.[10]

The stromal vascular fraction of homogenized adipose tissue is enriched in stem cells that have the capacity to accelerate repair of nonhealing skin wounds,[11–14] including a heterogeneous mixture of cell types such as endothelial progenitor cells, adipose-derived stem/stromal cells (ADSCs, predominantly mesenchymal stem/stromal cells), and pericytes. While the healing capacity of these cells may differ according to the specific cell type isolated from adipose and donor characteristics, such as body mass index, health status, and age,[14–17] studies suggest that ADSCs exhibit high potential for treating skin wounds in diabetic rodent models.[11–13,18] The extent to which stem cells from other tissues, including muscle-derived stem cells (MDSCs), exhibit a similar capacity for wound healing but has not been thoroughly evaluated.

Promising advances have been made in recent years in the development of stem cell therapy for nonhealing diabetic wounds.[19,20] However, most analyses and assessments of wound healing have been completed using standard photography, *in vitro* cell work, and histology. While these techniques offer invaluable information, the *in vivo* environment is more complicated, and it can be difficult to infer how a specific type of treatment will affect the microenvironment of the skin as a whole based solely on *in vitro* cell studies. In addition, due to the limited resolution of the photographs, a wound may appear "closed and healed," but the underlying collagen structures or vasculature networks are not fully remodeled. A surface-closed wound without a proper collagen structure underneath does not offer the same mechanical integrity as nonwounded skin and can be prone to further damage in the future. To address these issues, a technology capable of noninvasive, *in vivo* monitoring of wound healing with cellular-level resolution will provide a better understanding of this complex process, and the effect of treatments on different parts of the healing process in a natural environment. In recent years, several optical imaging techniques with high resolution have been utilized for wound healing assessment, including optical coherence tomography, confocal laser scanning microscopy (CLSM), hyperspectral imaging, and multiphoton microscopy (MPM).[21–24] These imaging techniques have provided both structural information and the healing dynamics of wounds at a scale that cannot always be obtained from visual observation and histology. MPM, including two-photon fluorescence (TPF) and second-harmonic generation (SHG) microscopy, is uniquely suited for probing the *in vivo* microenvironment of skin due to its noninvasive nature, label-free contrast mechanisms, and capacity for cellular-level resolution. TPF utilizes two-photon excitation at longer wavelengths to visualize both endogenous and exogenous fluorophores[25,26] while SHG is a label-free nonlinear optical technique that generates contrast from the noncentrosymmetric organization of molecules. SHG is often used to investigate collagen, a major constituent of the skin dermis.[25–27] By spatially and temporally coregistering TPF and SHG channels, the dynamic cellular activity in relation to collagen regeneration and reorganization during wound healing can be visualized.

In this longitudinal study, ADSCs and MDSCs[28] were applied to skin wounds of wild-type (WT) and diabetic mice. Stem cell localization and collagen remodeling were monitored *in vivo* during wound healing utilizing a custom-built MPM system equipped with TPF and SHG modalities. TPF was used to track the fluorescently labeled ADSCs and MDSCs, and SHG was used to monitor the changes in collagen organization during wound healing. The results from the technology used in this study provide new information regarding the basic process of skin wound repair, as well as insight regarding potential mechanisms by which stem cells contribute to the treatment of diabetic wounds.

2 Methods

2.1 *Animals, Skin Preparation, and Wounding*

All animal procedures were performed under protocols approved by the Institutional Animal Care and Use Committee (IACUC) at the University of Illinois at Urbana-Champaign. Both male BKS.Cg-Dock7m +/+ Leprdb/J (db/db) diabetic mice and male C57BL/6 WT mice (Jackson Laboratory, Bar Harbor, Maine) were used in this study. Before imaging, skin preparation and wounding were performed under anesthesia (1.5% isofluorane gas mixed with 2% oxygen). Hair on the lower dorsal skin was first shaved with electric clippers (Peanut palm size clipper 8652, Wahl), and the remaining hair in the region was further removed under a surgical microscope using surgical tweezers. The shaved skin was then cleaned with rubbing alcohol, and full thickness excisional wounds were made using a sterile 1 mm biopsy punch (Miltex, Inc., Miami, Florida). The wounded skin was then gently cleaned with rubbing alcohol.

2.2 *Stem Cell Isolation and Fluorescence-Activated Cell Sorting*

Stem cell isolation was performed under a laminar flow hood using sterile technique as previously reported.[29] Excised epididymal fat pads or gastrocnemius–soleus complexes were extensively minced in phosphate-buffered saline (PBS) and subjected to enzymatic digestions in 0.2% Type I collagenase (Worthington Biochemical Co., Lakewood, New Jersey) for 45 min with repeated trituration. After adding the inhibition solution [20% fetal bovine serum (FBS) in Hank's balanced salt solution (HBSS)] the samples were spun for 5 min at $450 \times g$ and filtered through a 70-μm strainer. The cells were then blocked with antimouse CD16/CD32 (eBioscience, San Diego, California) antibody for 10 min on ice to prevent nonspecific Fc receptor-mediated binding. Following the blocking step, cells were incubated with a fluorescent-conjugated antibody cocktail (Anti Sca-1-PE, 600 ng/10^6 cells and anti-CD45-APC, 300 ng/10^6 cells, eBioscience, San Diego, California) diluted in 2% FBS in PBS for 1 h on ice, followed by two washes in 2% FBS in PBS. Fluorescence-activated cell sorting (FACS) was performed on an iCyt Reflection System (iCyt, Urbana, Illinois) and Sca 1^+CD45^- cells were collected in growth media [high glucose Dulbecco's modified eagle's medium (DMEM), 10% FBS, 5 μg/mL gentamycin].

2.3 *Stem Cell Labeling and Injection*

FACS-isolated adipose- or muscle-derived Sca 1^+CD45^- cells were seeded on 100 mm plastic culture dishes (10^6 cells) and the growth media was changed every 3 to 4 days. MDSCs were previously characterized as $Pax7^-CD31^-CD34^-$ cells with multilineage potential.[28] After 8 days, cells were incubated for 10 min at 37°C with 5-mL StemPro Accutase Cell Dissociation Reagent (Life Technologies, Grand Island, New York). Equal volume of growth media was then added to

stop the dissociation reagent and cells were subjected to low speed centrifugation (5 min at $450 \times g$). The supernatant was discarded and the pellet was resuspended in 1-mL serum-free media (high glucose DMEM). Cells were then incubated for 20 min with 5-μL Vybrant DiI cell-labeling solution (Life Technologies, Grand Island, New York) at 37°C in the dark, followed by three washes with serum-free media. Cells were then resuspended in HBSS at 10^6 cells per 1 mL and were introduced into the wound perimeter using repeated subdermal injection (100 μL, 9×10^4 to 10^5 cells per wound). The skin around the wound site usually "bubbled up" after injection, which was an indication that cell suspension had been introduced.

2.4 *Multimodal Microscope*

Imaging of the skin was performed using a custom-built integrated MPM system described previously.[25,26] The system utilizes a tunable titanium:sapphire laser (Mai Tai HP, Spectra Physics) as the laser source. The center wavelength of excitation for both SHG and TPF imaging was 920 nm to achieve optical excitation of both the DiI-labeled stem cells and the endogenous collagen, and to remove unwanted background signal such as autofluorescence signals from other skin components.[30] The laser was directed through two scanning mirrors and the sample arm, and was focused onto the skin using a 0.95-NA objective lens (XLUMP20X, Olympus). The TPF and SHG signals were separated by a dichroic mirror and were simultaneously detected by two separated photomultiplier tubes (Fig. 1). With this system setup, spatial coregistration of TPF and SHG is achieved since the two types of signals are detected at the same time. The spatially coregistered MPM images can yield better insight into the relationship between the localization and cellular activity of stem cells and collagen structure during wound healing.[26,31]

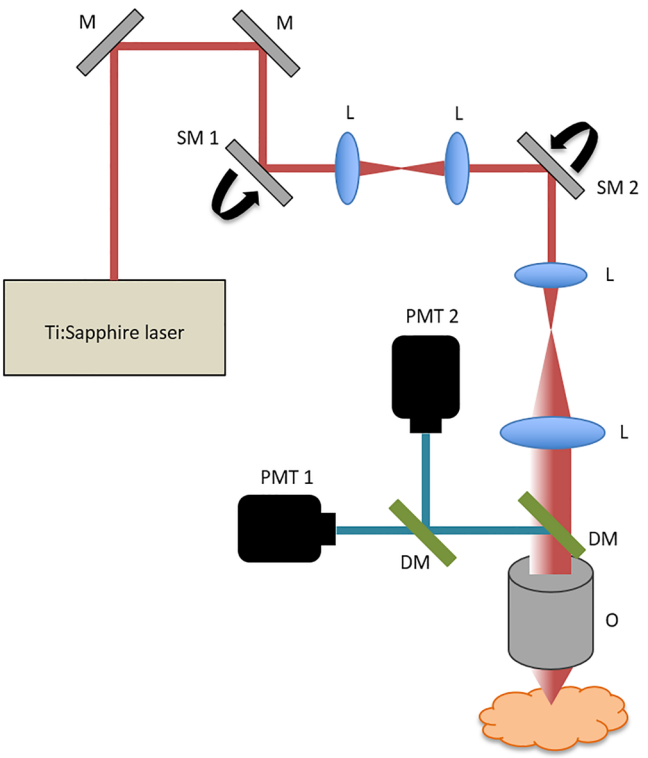

Fig. 1 Schematic of the MPM microscope system. M, mirror; SM, scanning mirror; L, lens; DM, dichroic mirror; O, objective; PMT, photomultiplier tube.

2.5 *Study Design*

Both diabetic mice ($n = 18$) and the WT mice ($n = 18$) were examined in this study. Each type of mouse was divided to three subgroups (six mice/group): no treatment (saline injection), ADSCs treatment, and MDSCs treatment. All six animals in each group were wounded on Day 0. Two of the six mice in each group were randomly chosen to be imaged using the multimodal microscope on Days 0 (after wounding), 1, 2, 4, and 8. The saline/stem cell injections were performed on Day 0 after imaging, and the wounds were covered with Tegaderm (3M, Indianapolis, Indiana) and surgical gauze to minimize animal scratching and photobleaching of the DiI-labeled cells. In addition to the microscope imaging, standard photographs of the wounds on all animals were acquired on each imaging day for comparison.

2.6 *Image Acquisition and Processing*

TPF and SHG images of the wounded skin were acquired concurrently with image dimensions of $\sim 2 \times 2$ mm^2 using a motorized stage to scan in the lateral dimensions. The position of the laser beam relative to the skin wound was used as a reference to ensure that the wound site and the same area of skin were captured within the field-of-view during scanning each day. Large-area images were assembled as mosaics of 10×10 individual images that were stitched together in postprocessing using MATLAB® (Mathworks) and ImageJ (National Institutes of Health). TPF and SHG images of the wounds were overlaid using ImageJ.

2.7 *Wound Size and Collagen Remodeling Measurements*

The size of wounds was measured in ImageJ from the photographs captured with a surgical microscope on each imaging day. The percent of wound closure was calculated by dividing the change in wound size compared to the initial wound size (Day 0) by the initial wound size.

To calculate the percent of collagen remodeling, segmentation of the SHG collagen images was performed using MATLAB®. Each SHG image was first converted to a binary image utilizing Otsu's method, and the wound bed and its area in each binary image can then be identified and measured. The percent of collagen remodeling was calculated using the same method as the percent of wound closure described above.

2.8 *Statistical Analysis*

All data are presented as means ± standard error (SE). Wound healing dynamics (changes in wound size based on photographs) were first evaluated for WT mice, and then repeated for diabetic mice. Two-way repeated measures ANOVA (5×3) were used to investigate main and combined effects of time (Days 0, 1, 2, 4, and 8) and treatment (saline control versus ADSCs versus MDSCs) on wound size, followed by Fisher's least significant difference *post hoc* analysis. Statistical analysis was performed using SPSS Ver. 20 (IBM, Chicago, Illinois). Differences were considered significant at $p \leq 0.05$. In addition, a nonparametric test was performed using Friedman's test

coupled with multiple comparison analysis, and the result was comparable to that from two-way repeated ANOVA.

3 Results

3.1 *Effect of Treatment in Wild-Type Mice*

After wounding, WT mice were randomly divided into three treatment groups (six per group): saline treatment (control), ADSC treatment, and MDSC treatment. Figure 2(a) shows the representative photographs of the wounded skin on Days 0, 2, 4, and 8, obtained using the surgical microscope. The area of skin that was considered part of the wound was identified with dashed lines in the photographs [Fig. 2(a)]. Good healing was observed in all three groups. However, a better healing trend was observed in cell-treated groups compared to the saline treatment group [Fig. 2(b)], and the percent wound closure of both cell-treated groups was significantly higher than the saline group on Day 2 [Fig. 2(b), ADSCs: $p \leq 0.01$; MDSCs: $p \leq 0.05$].

Two of the six animals in each group were randomly chosen for imaging utilizing the MPM system. Composite images of SHG and TPF illustrate the progression of collagen remodeling (SHG) and the localization of ADSCs and MDSCs (TPF) during the course of study (Fig. 3). Collagen matrix remodeling was observed in all three treatment groups. However, a more organized collagen network, consisting of stronger SHG signals as well as a "basket-weave" structural organization associated with normal skin,[6] was readily apparent in the stem-cell treated groups compared to the saline control groups [Fig. 3(a)]. A collagen network with the "basket-weave" structure would be mechanically stronger and provide better structural support than a collagen network without this type of structure.[6] This observation was most evident on Days 4 and 8, as both cell-treated groups demonstrated visible collagen contraction around the wound bed. In addition, the TPF fluorescence signal from stem cells was visible in both cell-treated groups, and ADSCs and MDSCs appeared to remain close to the edge and center of

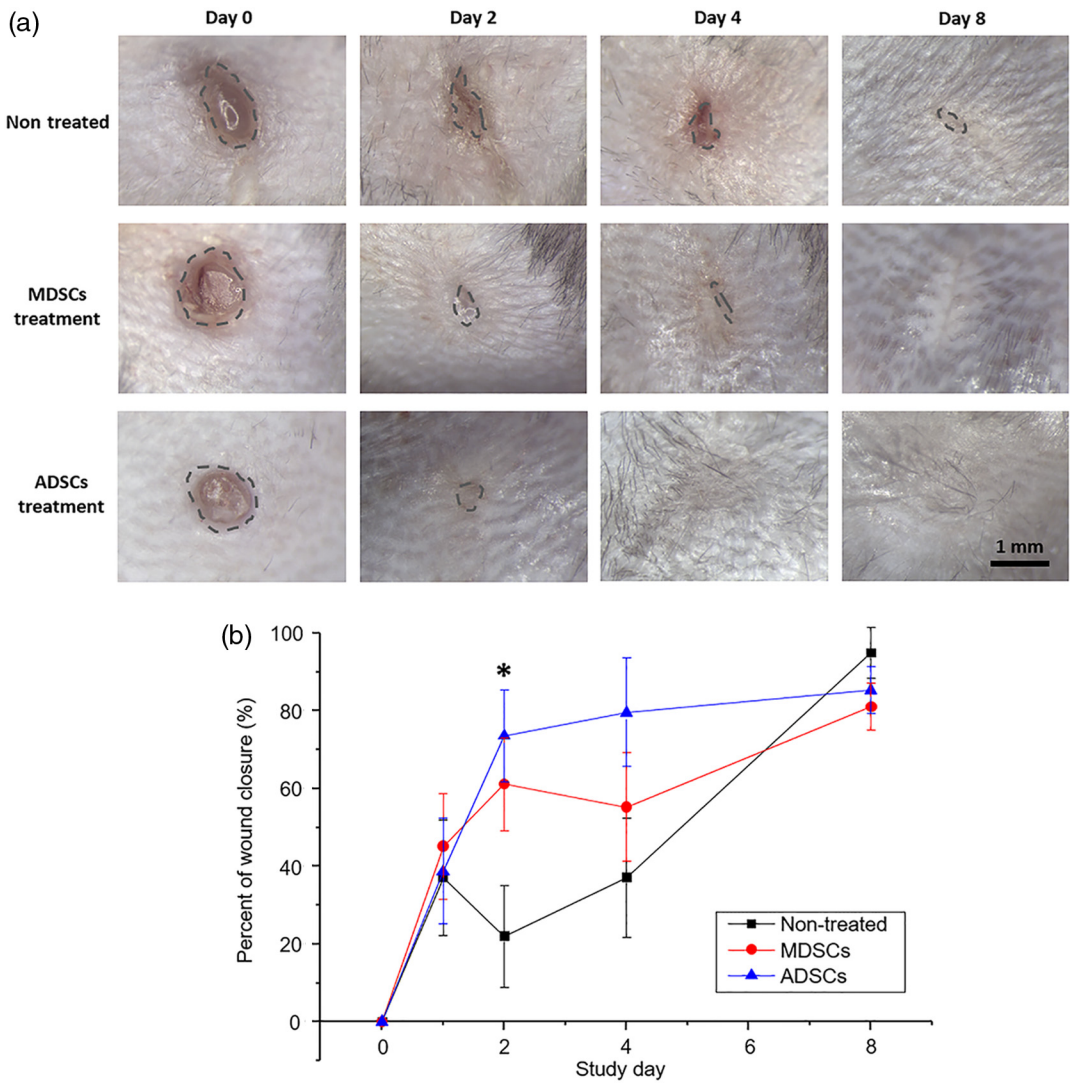

Fig. 2 Wound size comparison across all treatment groups in WT mice. (a) Representative photographs of the wounded skin in each treatment group on Days 0, 2, 4, and 8. Area of the skin that is considered part of the wound was identified by dashed line. Scale bar: 1 mm applies to all photos. (b) Comparison of the percent of wound closure measured from the photographs ($n = 6$, mean $\pm$ SE). *On Day 2, the percentage wound closure of nontreated group was significantly lower than both ADSCs treatment group ($p \leq 0.01$) and MDSCs treatment group ($p \leq 0.05$).

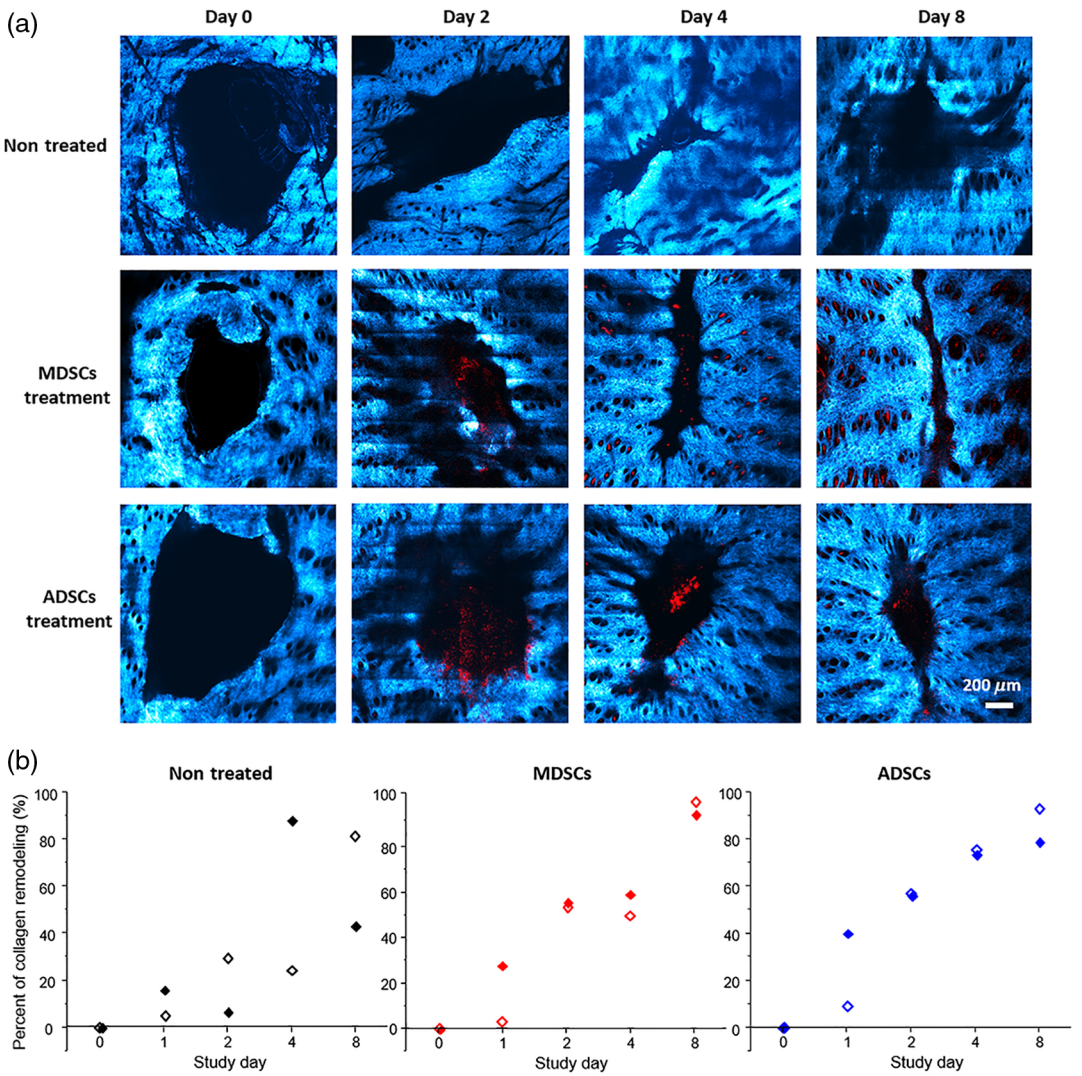

Fig. 3 Comparison of collagen remodeling and dynamic movement of stem cells in all three groups of WT mice. DiI-labeled stem cells were administered after imaging on Day 0, and two out of six mice from each treatment group were selected for MPM imaging. (a) Representative composite MPM images of the collagen matrix (SHG, blue), and the DiI-labeled stem cells (TPF, red) of the wounded skin in each treatment group on Days 0, 2, 4, and 8. Scale bar: 200 μm applies to all images. (b) Comparison of the percentage collagen remodeling calculated using the SHG images ($n = 2$, solid dot: animal #1; hollow dot: animal #2). Both treated groups showed slightly faster rate of collagen remodeling compared to nontreated group.

the wound during most of the healing. Finally, the rate of healing was assessed by quantifying the percent of collagen remodeling (see Sec. 2.7). The rate of collagen remodeling in the wound was slightly faster in both cell-treated groups compared to the saline controls, shown by the faster rise of dynamic trends [Fig. 3(b)]. The MPM results reflect a similar trend as wound closure measurements obtained by traditional photography [Fig. 2(b)], but offering additional new high-resolution subsurface visualization of the collagen network.

3.2 *Effect of Treatment in Diabetic (db/db) Mice*

Db/db mice were also randomly divided into three groups and received the same treatments as WT mice. As observed in the photographs of the wounded skin, the wound size increased in *db/db* mice without treatment (control) on Days 2 and 4, and the skin around the wound bed appeared to deteriorate with skin reddening [Fig. 4(a)]. In contrast, both stem cell-treated groups showed a progressive decrease in the wound size [Fig. 4(a)]. The percent of wound closure was also calculated. One day following treatment (Day 1), the average wound size was significantly smaller in the group treated with MDSCs compared to the saline group [Fig. 4(b), $p \leq 0.05$]. Wound size was significantly smaller in both cell-treated groups two days post-treatment [Fig. 4(b), $p \leq 0.05$ for ADSCs and $p \leq 0.01$ for MDSCs], and remained smaller 4 and 8 days post-treatment [Fig. 4(b), $p \leq 0.01$ for both cell types].

Two of the six animals from each group were randomly selected for imaging with the MPM system. While the nontreated diabetic mice exhibited increased wound size during the first 4 days, immediate and progressive healing was observed in the stem cell-treated groups (Fig. 5). TPF signal was recorded inside the wound bed in both cell-treated groups [Fig. 5(a)]. Stem cells appeared to be localized to the center of the

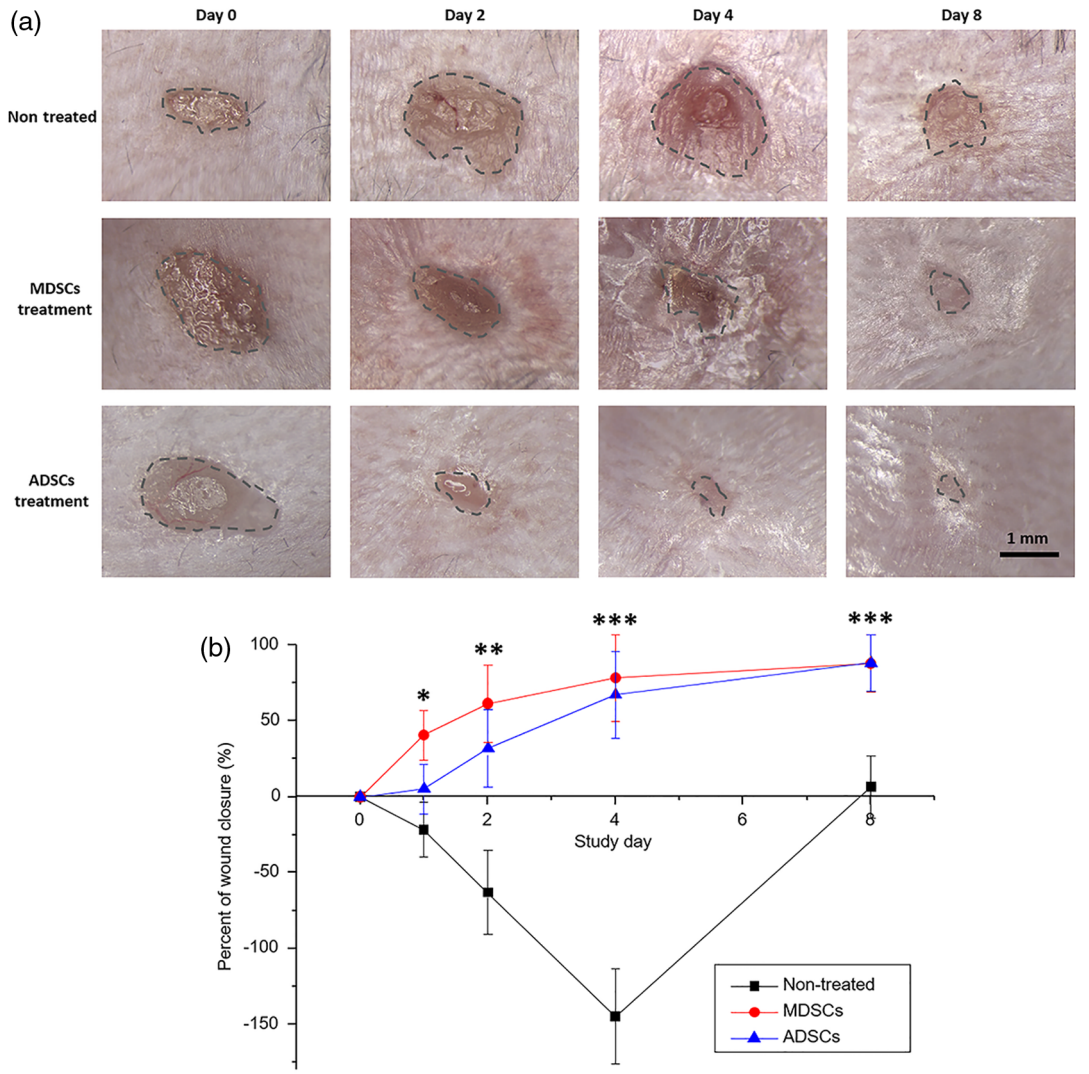

Fig. 4 Wound size comparison across all treatment groups in *db/db* mice. (a) Representative photographs of the wounded skin in each group on Days 0, 2, 4, and 8. Area of the skin considered as part of the wound was identified by dashed lines. Scale bar: 1 mm applies to all. (b) Comparison of the percent of wound closure from all three groups of mice measured from the photographs ($n = 6$, mean ≅ SE). * On Day 1, the percent wound closure of nontreated group was significantly lower than MDSCs treatment group ($p \leq 0.05$). ** On Day 2, the percent wound closure of nontreated group was significantly lower than both ADSCs treatment group ($p \leq 0.05$) and MDSCs treatment group ($p \leq 0.01$). *** On Days 4 and 8, the percent wound closure of nontreated group was significantly lower than both ADSCs and MDSCs treatment groups ($p \leq 0.01$).

wound bed. Quantitative data obtained from the MPM images [Fig. 5(b)] reflected comparative results from the photographs [Fig. 4(b)]. However, it appeared that the collagen matrix remodeled at a slower rate than the actual wound closure [Figs. 4(b) and 5(b)]. In addition, by further comparing the photographs [Fig. 4(a)] and the SHG images [Fig. 5(a)], it was observed that the darker and reddened skin around the edge of wounds, seen in the photographs, corresponds to areas with minimal or no collagen signal. This observation is shown in Fig. 6, which again emphasizes the importance of having subsurface information to fully understand the condition of the healing skin.

Closer examination of the wound bed revealed colocalization of fluorescently labeled stem cells with collagen fibril network in both WT and *db/db* mice (representative image for *db/db* mouse shown in Fig. 7, indicated with arrows). The observation suggests the capacity for stem cells to attach to and/or remodel the ECM. In addition, Fig. 7 shows that MPM imaging provides the level of *in vivo* subsurface details of the skin microenvironment that cannot be observed in standard photographs.

4 Discussion

ADSCs demonstrate significant capacity for healing in multiple tissues in humans and animal models.[10] The purpose of the current study was to microscopically visualize, quantify, and determine the impact of topically applied stem cells isolated from adipose and skeletal muscle on diabetic wound healing. Both ADSCs and MDSCs exhibited remarkable and equivalent capacity to repair diabetic wounds, likely due to their ability to synthesize and replace multiple growth, angiogenic, and immunomodulatory factors deficient in the diabetic wound bed. The application of our unique imaging system for the

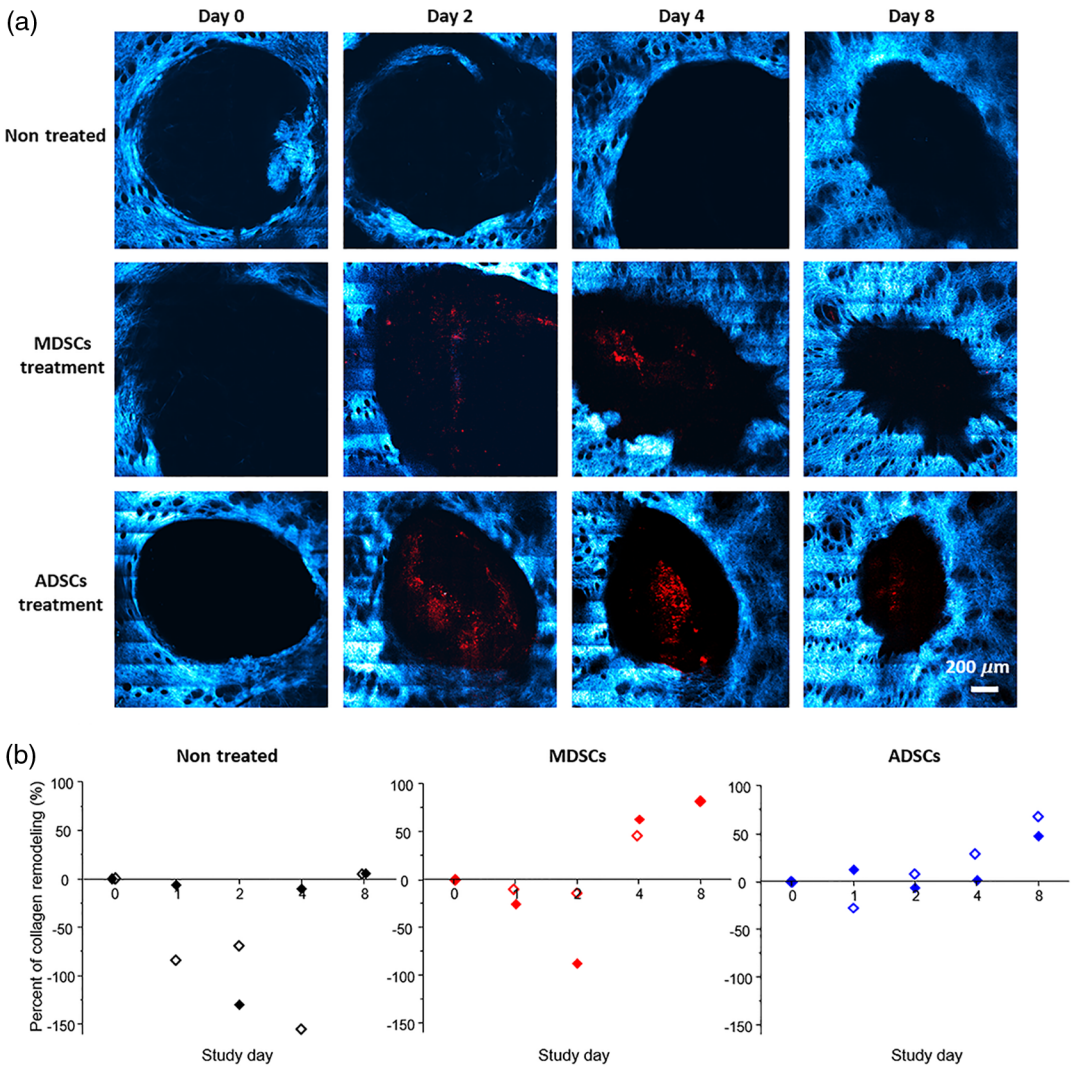

Fig. 5 Comparison of collagen remodeling and dynamic movement of stem cells in all three groups of *db*/*db* mice. DiI-labeled stem cells were administered after imaging on Day 0, and two out of six mice from each treatment group were selected for MPM imaging. (a) Representative composite MPM images of the collagen matrix (SHG, blue) and the DiI-labeled stem cells (TPF, red) of the wounded skin in each treatment group on Days 0, 2, 4, and 8. Scale bar: 200 μm applies to all images. (b) Comparison of the percentage collagen remodeling calculated using the SHG images ($n = 2$, solid dot: animal #1; hollow dot: animal #2). Both treated groups showed noticeably faster rate of collagen remodeling compared to nontreated group. The nontreated group showed an increase in wound size during the study, and there were minimal changes in wound size on Day 8 compared to Day 0.

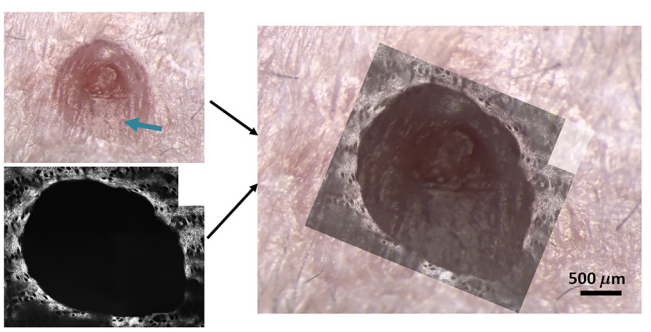

Fig. 6 Overlay of the standard photograph and SHG image from the nontreated mouse on Day 4, which shows the lack of SHG signals in the reddened skin seen in the photograph (blue arrow). Scale bar: 500 μm.

assessment of wound repair revealed interesting insight regarding stem cell localization and influence on structural remodeling at the site of injury. The results from this study provide further justification for stem cell-based therapeutics and the potential of MPM for assessment of wound healing in diabetic patients.

The use of traditional histology for visualizing and evaluating the process of wound healing is significantly limited given the complexity of cellular events within the skin microenvironment. Recent advances in optical microscopy technologies, such as with reflectance microscopy or CLSM, provide increased capacity for imaging cell dynamics in skin during normal or pathological conditions.[32,33] However, these imaging modalities do not typically provide both spatial and temporal coregistration in a multimodal imaging setting. A solution to this challenge has been to develop an integrated multimodal microscope that combines the various mechanisms of physical contrast from cells

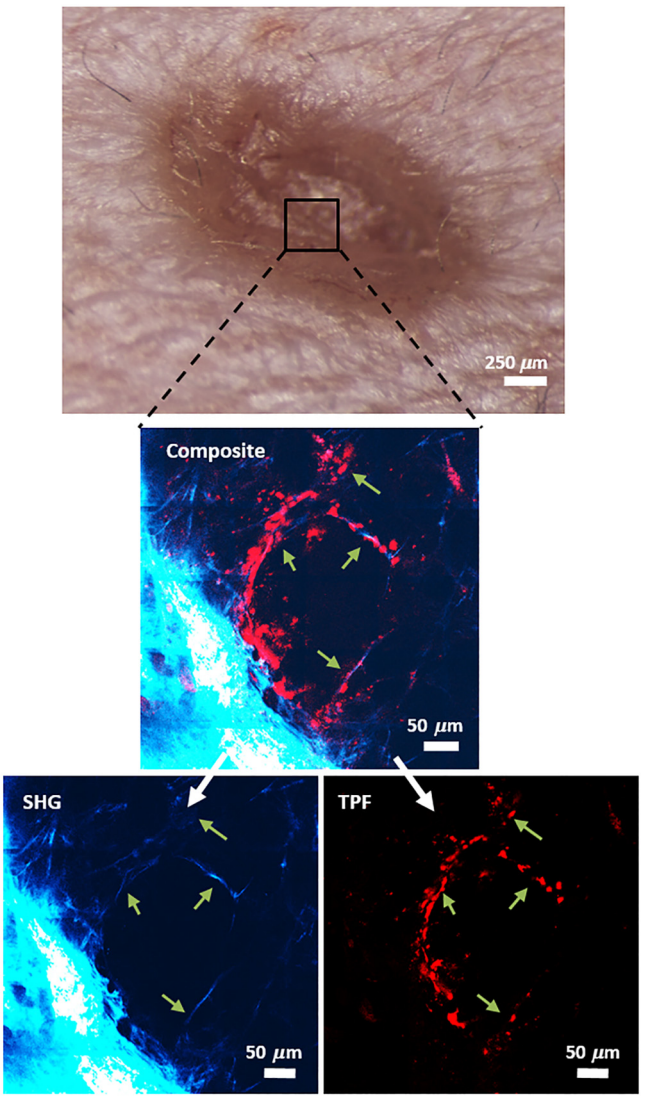

Fig. 7 Microscopic visualization of collagen network remodeling and cellular dynamics in treated *db/db* mice. In the SHG and TPF images acquired at the area indicated in the photograph (black box), locations where visible colocalization of collagen fibers and stem cells were identified (green arrows in MPM images). Scale bars: photograph 250 μm; MPM images: 50 μm.

and tissues as well as to implement registration algorithms to longitudinally track cell, tissue, and microvascular dynamics in skin injury and regeneration over weeks to months.[26]

It is clear from both photographic and MPM images provided in this study that diabetic mice treated with stem cells exhibited significantly faster wound closure rates than mice that did not receive treatment. While standard photography captured the process of wound closure, it did not provide the microscopic subsurface information necessary to reveal stem cell localization or the impact of the stem cells on the surrounding environment. The example comparison of photographic and MPM images in Fig. 7 shows the level of *in vivo* resolution in MPM images that photography cannot offer. Coregistration of the SHG and TPF channels allows visualization of thin collagen fibers on the edge of the wound bed, as well as the individual stem cells that interact with the collagen fibers. This observation could suggest that the stem cells applied to the wounded skin anchored onto these loose collagen fibers to migrate or to communicate with the host cells, or that the stem cells were directly involved in collagen remodeling at the edge of the wound.[34,35] The relationship between these stem cells and collagen remodeling during healing should be further investigated and explored, and larger imaging sample size is needed in future studies to achieve higher statistical power, and to evaluate the reliability of this imaging technology in assessing wound treatments.

Impaired diabetic wound healing is the accumulated result of numerous complications and abnormalities, including decreased collagen synthesis and insufficient neovascularization. These two processes are heavily dependent on each other since the ECM provides the tissue foundation for vascularization, and newly formed vessels deliver the oxygen and nutrients necessary for the healing process.[5,36] The mechanism by which the stem cells facilitated collagen synthesis in the current study is not clear, but stem cells are endowed with the capacity to synthesize both ECM proteins and metalloproteinases necessary for active tissue remodeling.[10,37] The contribution of topically applied stem cells to ECM turnover may provide the basis for the improved collagen remodeling observed in our MPM images. A strong collagen network that was actively contracting around the wound bed was clearly evident in stem cell-treated mice, including WT mice that appeared to heal effectively based on photographic images. Although not directly assessed in this study, it is possible that enhancement of collagen remodeling and structure provides the basis for protection from further damage and/or long-term scarring. Therefore, stem cell administration may be advantageous for healthy individuals, as well as individuals in which endogenous stem cell migration and function may be lacking.

5 Conclusions

In this study, preliminary results demonstrated our integrated MPM imaging as a promising technology to investigate complex biological processes in wound healing and to assess new wound healing treatments. While standard photography and *ex vivo* analysis can shed light on the healing rate and the final pathological conditions of the skin, wound healing is a highly dynamic process, and having a technology capable of performing *in vivo* longitudinal tracking of skin conditions at cellular-level resolution is imperative. To better understand the potential of this technology in characterizing diabetic wound healing and treatments, additional studies are necessary such as examining time-lapse three-dimensional cell dynamics and future *in vivo* human studies. Furthermore, a longer follow-up period postwounding should be implemented in future studies in order to capture the complete healing process.

Stem cell transplantation offers an important therapeutic approach to the treatment of nonhealing diabetic wounds. In order to assess the strengths of this approach, MPM imaging represents a significant advancement in the ability to visualize and understand the biological basis for healing, as well as the capacity to assess regenerative therapies in patients that suffer from painful and debilitating nonhealing wounds.

Acknowledgments

We thank Darold Spillman (University of Illinois at Urbana-Champaign) for assistance with logistical and information technology support. This research was supported in part by grants from the National Institutes of Health (1 R01 EB013723 and

1 R01 CA166309). JL was supported in part by the Beckman Institute Graduate Fellowship (Beckman Institute for Advanced Science and Technology) and a Support for Under-Represented Groups in Engineering (SURGE) Fellowship (University of Illinois at Urbana-Champaign). AJB was supported by the National Science Foundation Graduate Research Fellowship Program (DGE-1144245). Additional information can be found at http://biophotonics.illinois.edu.

References

1. American Diabetes Association, www.diabetes.org.
2. F. Giacco and M. Brownlee, "Oxidative stress and diabetic complications," *Circ. Res.* **107**(9), 1058–1070 (2010).
3. J. M. Forbes and M. E. Cooper, "Mechanisms of diabetic complications," *Physiol. Rev.* **93**(1), 137–188 (2013).
4. V. Falanga, "Wound healing and its impairment in the diabetic foot," *Lancet* **366**(9498), 1736–1743 (2005).
5. A. J. Singer and R. A. Clark, "Cutaneous wound healing," *N. Engl. J. Med.* **341**(10), 738–746 (1999).
6. M. B. Witte and A. Barbul, "General principles of wound healing," *Surg. Clin. North Am.* **77**(3), 509–528 (1997).
7. T. Velnar, T. Bailey, and V. Smrkoli, "The wound healing process: an overview of the cellular and molecular mechanisms," *J. Int. Med. Res.* **37**(5), 1528–1542 (2009).
8. J. Li, J. Chen, and R. Kirsner, "Pathophysiology of acute wound healing," *Clin. Dermatol.* **25**(1), 9–18 (2007).
9. R. F. Diegelmann and M. C. Evans, "Wound healing: an overview of acute, fibrotic and delayed healing," *Front Biosci.* **9**, 283–289 (2004).
10. B. M. Dulmovits and I. M. Herman, "Microvascular remodeling and wound healing: a role for pericytes," *Int. J. Biochem. Cell Biol.* **44**(11), 1800–1812 (2012).
11. M. Nambu et al., "Accelerated wound healing in healing-impaired db/db mice by autologous adipose tissue-derived stromal cells combined with atelocollagen matrix," *Ann. Plast. Surg.* **62**(3), 317–321 (2009).
12. M. K. Maharlooei et al., "Adipose tissue derived mesenchymal stem cell (AD-MSC) promotes skin wound healing in diabetic rats," *Diabetes Res. Clin. Pract.* **93**(2), 228–234 (2011).
13. C. L. Nie et al., "Locally administered adipose-derived stem cells accelerate wound healing through differentiation and vasculogenesis," *Cell Transplant* **20**(2), 205–216 (2011).
14. L. Zimmerlin et al., "Mesenchymal markers on human adipose stem/progenitor cells," *Cytometry* **83A**(1), 134–140 (2013).
15. L. Aust et al., "Yield of human adipose-derived adult stem cells from liposuction aspirates," *Cytotherapy* **6**(1), 7–14 (2004).
16. C. S. Lin et al., "Defining adipose tissue-derived stem cells in tissue and in culture," *Histol. Histopathol.* **25**(6), 807–815 (2010).
17. L. Zimmerlin et al., "Stromal vascular progenitors in adult human adipose tissue," *Cytometry, Part A* **77A**(1), 22–30 (2010).
18. L. Zimmerlin et al., "Human adipose stromal vascular cell delivery in a fibrin spray," *Cytotherapy* **15**(1), 102–108 (2013).
19. J. Xu et al., "The role of microRNA-146a in the pathogenesis of the diabetic wound-healing impairment: correction with mesenchymal stem cell treatment," *Diabetes* **61**(11), 2906–2912 (2012).
20. A. O'Loughlin et al., "Topical administration of allogeneic mesenchymal stromal cells seeded in a collagen scaffold augments wound healing and increases angiogenesis in the diabetic rabbit ulcer," *Diabetes* **62**(7), 2588–2594 (2013).
21. S. Lange-Asschenfeldt et al., "Applicability of confocal laser scanning microscopy for evaluation and monitoring of cutaneous wound healing," *J. Biomed. Opt.* **17**(7), 076016 (2012).
22. M. Kuck et al., "Evaluation of optical coherence tomography as a non-invasive diagnostic tool in cutaneous wound healing," *Skin Res. Technol.* **20**(1), 1–7 (2014).
23. M. A. Calin et al., "Characterization of burns using hyperspectral imaging technique—a preliminary study," *Burns* **41**(1), 118–124 (2015).
24. J. Li et al., "Effect of recombinant interleukin-12 on murine skin regeneration and cell dynamics using in vivo multimodal microscopy," *Biomed. Opt. Express* **6**(11), 4277–4287 (2015).
25. B. W. Graf et al., "In vivo multimodal microscopy for detecting bone-marrow-derived cell contribution to skin regeneration," *J. Biophotonics* **7**(1-2), 96–102 (2014).
26. B. W. Graf et al., "Long-term time-lapse multimodal intravital imaging of regeneration and bone-marrow-derived cell dynamics in skin," *Technology* **1**(1), 8–19 (2013).
27. P. J. Campagnola and L. M. Loew, "Second-harmonic imaging microscopy for visualizing biomolecular arrays in cells, tissues and organisms," *Nat. Biotechnol.* **21**(11), 1356–1360 (2003).
28. M. C. Valero et al., "Eccentric exercise facilitates mesenchymal stem cell appearance in skeletal muscle," *PLoS One* **7**(1) (2012).
29. K. Zou et al., "Laminin-111 improves skeletal muscle stem cell quantity and function following eccentric exercise," *Stem Cells Transl. Med.* **3**(9), 1013–1022 (2014).
30. H. G. Breunig, H. Studier, and K. Konig, "Multiphoton excitation characteristics of cellular fluorophores of human skin in vivo," *Opt. Express* **18**(8), 7857–7871 (2010).
31. A. Zoumi, A. Yeh, and B. J. Tromberg, "Imaging cells and extracellular matrix in vivo by using second-harmonic generation and two-photon excited fluorescence," *Proc. Natl. Acad. Sci. U. S. A.* **99**(17), 11014–11019 (2002).
32. M. Ulrich and S. Lange-Asschenfeldt, "In vivo confocal microscopy in dermatology: from research to clinical application," *J. Biomed. Opt.* **18**(6), 061212 (2013).
33. D. S. Gareau et al., "Rapid screening of cancer margins in tissue with multimodal confocal microscopy," *J. Surg. Res.* **178**(2), 533–538 (2012).
34. B. Gharaibeh et al., "Terminal differentiation is not a major determinant for the success of stem cell therapy—cross-talk between muscle-derived stem cells and host cells," *Stem Cell Res. Ther.* **2**(4), 31 (2011).
35. W. S. Kim et al., "Wound healing effect of adipose-derived stem cells: a critical role of secretory factors on human dermal fibroblasts," *J. Dermatol. Sci.* **48**(1), 15–24 (2007).
36. M. A. M. Loots et al., "Differences in cellular infiltrate and extracellular matrix of chronic diabetic and venous ulcers versus acute wounds," *J. Invest. Dermatol.* **111**(5), 850–857 (1998).
37. H. Gerhardt and C. Betsholtz, "Endothelial-pericyte interactions in angiogenesis," *Cell Tissue Res.* **314**(1), 15–23 (2003).

Joanne Li received her BS degree in chemical engineering from the University of Washington in 2011 and her MS degree in nuclear, plasma, and radiological engineering from the University of Illinois at Urbana-Champaign in 2013. She is currently a PhD student in bioengineering at the University of Illinois at Urbana-Champaign. She is currently a Beckman graduate fellow and research assistant in the Biophotonics Imaging Laboratory at Beckman Institute for Advanced Science and Technology.

Yair Pincu received his B Ed degree in physical education from Kaye College, Israel, in 2003, his MA degree in gerontology from Ben-Gurion University of the Negev, Israel, in 2007, and his PhD degree in exercise physiology from the University of Illinois at Urbana-Champaign in 2016. He was the recipient of the Fulbright doctoral fellowship from 2009 to 2011. He is currently a postdoctoral fellow in the cardiovascular biology research program in Oklahoma Medical Research Foundation.

Marina Marjanovic is currently an associate director of the Center for Optical Molecular Imaging and an adjunct associate professor in the Department of Bioengineering, University of Illinois at Urbana-Champaign. She received her BS degree in molecular biology and physiology in 1979, and her MS and PhD degrees in physiology, in 1987 and 1992, respectively, from the University of Belgrade, Serbia. Her research interests include physiological studies, especially those with medical relevance, using optical imaging technologies.

Andrew J. Bower received his BS degree in optical engineering and physics from Rose-Hulman Institute of Technology in 2012, and his MS degree in electrical and computer engineering from the University of Illinois at Urbana-Champaign in 2014. He is currently a PhD candidate in electrical and computer engineering at the University of Illinois at Urbana-Champaign and a member of the Biophotonics Imaging Laboratory at Beckman Institute for Advanced Science and Engineering.

Eric J. Chaney received his BS degree in biology from the University of Evansville in 1992. From 1993 to 1997, he was a research assistant at the Indiana University School of Medicine, Indiana State University. From 1997 to 2000, he was a transmission electron microscope technician at the University of Illinois at Urbana-Champaign. Since 2000, he has been a research scientist at the Biophotonics Imaging Laboratory, Beckman Institute for Advanced Science and Technology.

Tor Jensen is the laboratory director of the Biomedical Research Center at the Mills Breast Cancer Institute at Carle Foundation Hospital, Urbana, Illinois, USA. He received his BChE degree in chemical engineering at the University of Minnesota in 1997 and his PhD in chemical and biomolecular engineering at Northwestern University in 2004.

Marni D. Boppart is currently an associate professor in the Department of Kinesiology and Community Health, and the principal investigator of the Molecular Muscle Physiology Laboratory at the University of Illinois at Urbana-Champaign. She received her BS degree in molecular, cellular, and developmental biology from the University of New Hampshire in 1992, the MS degree in cell biology from Creighton University in 1996, and her ScD degree in applied anatomy and physiology from Boston University.

Stephen A. Boppart is currently an Abel Bliss professor of engineering in the Departments of Electrical and Computer Engineering, Bioengineering, and Medicine at the University of Illinois at Urbana-Champaign. He received his BS in electrical and bioengineering in 1990 and his MS in electrical engineering in 1991 from the University of Illinois at Urbana-Champaign, his PhD in electrical and medical engineering from the Massachusetts Institute of Technology (1998), and his MD from Harvard Medical School in 2000.